Design of Double Decoupled Phase-Locked Loop of Microgrid and Smooth Switching Control Strategy for On-grid and Off-grid Connection

Xin-Feng Du, Shuang Zhao, Jie-Sheng Wang *, An He

Abstract—**The control methods of microgrid are generally divided into micro-source level control, system level control and scheduling level control. Based on the equivalent structure of the AC microgrid, the transient mode of the AC microgrid switched from off-grid to grid-connected is proposed, the dual-decoupled phase-locked loop of the microgrid and the smooth control strategy switching from grid-connected to off-grid are proposed. The phase-locked loop is a key link for extracting the voltage amplitude, frequency and phase of the grid. In the case of grid voltage asymmetry, the phase-locking accuracy of the traditional phase-locked loop is insufficient. Under the grid voltage distortion state, the accuracy of the extracted grid voltage phase, amplitude and frequency is poor. A new phase-locked loop structure based on double decoupling is adopted so as to eliminate the double frequency disturbance of the grid voltage and improve the tracking accuracy of the phase-locked loop. The voltage amplitude, frequency and phase are the three key parameters switching from grid-connected to off-grid. So a new grid-connected pre-synchronization controller consisting of voltage regulator, frequency regulator and phase regulator is designed. The voltage and frequency operating values at the AC bus-bar divide the microgrid operation into four intervals, which can be better used to judge the switching condition between off-grid and grid-connected of the microgrid. The simulation experiments show that the proposed dual-decoupled phase-locked loop and the off-grid and grid-connected smooth switching control strategy of the microgrid can effectively reduce voltage impact of microgrid during off-grid and grid-connected switching process.**

Index Terms—**AC microgrid; Double decoupled phase-locked loop; smooth switching from grid-connected to off-grid**

Manuscript received August 24, 2019; revised October 21, 2019. This work was supported by the Basic Scientific Research Project of Institution of Higher Learning of Liaoning Province (Grant No. 2017FWDF10), and the Project by Liaoning Provincial Natural Science Foundation of China (Grant No. 20180550700).

Xin-Feng Du is a postgraduate student in the School of Electronic and Information Engineering, University of Science and Technology Liaoning, Anshan, 114051, PR China (e-mail: 13569510917@163.com).

Shuang Zhao is an engineer of Anshan Power Supply Company, State Grid Liaoning Electric Power Co. LTD., Anshan, 114051, PR China (e-mail: 857111565@qq.com).

Jie-Sheng Wang is with the School of Electronic and Information Engineering, University of Science and Technology Liaoning, Anshan, 114051, PR China; National Financial Security and System Equipment Engineering Research Center, University of Science and Technology Liaoning. (Corresponding author, phone: 86-0412-2538355; fax: 86-0412-2538244; e-mail: wang_jiesheng@126.com).

An He is an engineer of Anshan Power Supply Company, State Grid Liaoning Electric Power Co. LTD., Anshan, 114051, PR China (e-mail: 54hean@163.com).

I. Introduction

Energy is an important material basis for social development, and reliable power supply is crucial to supporting the building of modern civilization. Electricity is the most important secondary energy. Primary energy is converted into secondary energy in the form of electric energy, and is sent to the user side as a final-purpose energy source by various substations and transmission and distribution networks [1]. At present, the global energy Internet promoted by the State Grid Corporation is becoming an important comprehensive intelligent electrical platform for China to promote the upgrading of energy industry, high-technology power equipment construction and advanced power grid control optimization technology. The energy Internet not only contains traditional power systems, but also advanced power electronic power systems [2]. Energy Internet is a comprehensive ecological energy system with multiple energy participation and user-led intelligence, information and modulation. The intermittent and volatility of renewable energy power generation equipment will be adjusted and stabilized by power electronic equipment and energy storage equipment, which will enable the distributed power generation equipment to participate in power interaction. Since a high proportion of new energy is connected to the power system, the operating characteristics and control methods of the power system will be significantly different from the past, and this will bring a series of new scientific and technical problems. Considering the operating characteristics of distributed generation equipment, especially its uncertainty and randomness, electromagnetic coupling, power flow calculation, load estimation and relay protection of power systems will be the hot spots of future research [3]. The energy Internet will be a highly integrated information system and physical system, involving big data and cloud computing, so the energy Internet will be one of the most complex network organizations in human history. The energy Internet embodies a high degree of energy integration, and cross-regional connectivity and muti-energy access will become more common.

The structure of the microgrid depends on how the distributed generation equipment and load are connected to the AC and DC bus of the microgrid system. The microgrid can be divided into AC hybrid, DC hybrid, and AC/DC hybrid microgrid. In an AC hybrid microgrid, various

distributed power generation units and renewable energy units are connected to the AC bus through their power interface converters [4]. Renewable energy units require bidirectional converters to provide bidirectional power flow capability [5]. In this configuration, the AC and DC loads are also connected to a common bus, typically through a power electronic converter. This type of structure is typically used to generate a power frequency AC voltage through an interface power converter in a dominant power supply in a microgrid. In such an AC hybrid system, the control strategy and power management scheme are mainly focused on the power consumption balance and the AC bus voltage frequency control, especially in the off-grid operation mode. The AC hybrid microgrid is the current mainstream structure in that its structure is simple, and bus-bar control and power management are simple to implement. Thus, the entire system can be viewed as a single power processing unit with multiple interface ports.

For the operation of AC/DC hybrid microgrid, the microgrid control strategy and power management scheme are the most important research directions. The power management strategy determines the active and reactive power of the distributed generation unit and the renewable energy unit, while adjusting the voltage and frequency [6]. The AC hybrid microgrid control strategies can be divided into grid-connected control strategies and off-grid control strategies [7]. In the grid-connected mode, the power management strategy can be divided into a dispatch power mode and an unassigned output power mode. In the assigned output power mode, the microgrid behaves like a controllable source or main load and can provide valuable grid support or load management as a whole [8]. In this mode, the distributed generation unit and the renewable energy unit operate in the power control mode [9]. Power control can be achieved by current control or voltage control. The current control mode is currently used in the grid-connected operation control mode to control the output current of the distributed power generation unit and the renewable energy unit so as to track the grid of the reference power, output voltage and frequency [10]. In the voltage control mode, both the distributed generation unit and the renewable energy unit can control the output voltage, and the behavior of adjusting the distributed device output power is similar to that of the synchronous generator in the power system [11].

In the off-grid mode, the power management strategy of the microgrid mainly includes voltage regulation, frequency adjustment, reactive power regulation and active regulation [12]. The microgrid generally has one or more dominant nodes for voltage and frequency adjustment of the microgrid to ensure that the voltage and frequency operate in a stable interval [13]. The secondary regulation of frequency and voltage can pull the voltage and frequency of the microgrid from the edge of collapse to the stable operating range, which enhances the stability of the microgrid [14]. The regulation of reactive power and active power are the basis for ensuring the stability of the microgrid voltage and frequency. In generally the control of reactive power is the hot spot of microgrid off-grid operation mode [15]. In addition, the switching strategy of off-grid and grid-connected is also an important research point to ensure the synchronization of the microgrid and the main grid voltage, frequency and phase, which can improve the stability of the microgrid and the main grid connection, and improve the system's power optimal allocation [16]. In the off-grid mode, reactive power sharing is an important adjustment to ensure the stability of the microgrid voltage. The general reactive power sharing strategy is usually divided into communication-based reactive power regulation and communication-free reactive power regulation [17]. Based on the reactive power regulation of communication, there is a dominant node in the system, and the sharing control of reactive power is realized through interactive communication. The non-communication reactive power sharing strategy has good communication stability and cost control, but its general control strategy is more complicated, and it also needs to ensure the stable operation of the microgrid through hierarchical control [18].

The control methods of the microgrid are generally divided into micro-source level control, system level control, and scheduling level control. The micro-source level control is mainly to ensure the stability of the micro-source operation, including adjusting the output voltage, frequency and active and reactive power of the micro-source. System-level control generally ensures stable operation of the microgrid system, generally based on voltage and frequency regulation at the AC bus, improving the operational stability of the system [19]. Scheduling-level control is to ensure the optimal use of energy in the entire microgrid system, generally using optimization algorithms and considering system economics [20]. In this paper, the system equivalent structure of AC microgrid is studied. The structure design of AC decoupling phase-locked loop and the smooth control strategy of grid-connected and off-grid are proposed and verified by simulation. The structure of the paper is described as follows. Second 2 introduces the simplified structure of the microgrid muti-energy system. Section 3 introduces the microgrid phase-locked loop design. Section 4 is the off-grid and grid-connected switching strategy. Section 5 is the operating conditions division of microgrid off-grid and grid-connected. Section 6 is the experimental simulation and result analysis. Finally is the conclusion of the paper.

II. Simplified Structure of Microgrid Multiple Energy System

The key of the stable operation of the microgrid system is to ensure that the voltage and frequency of the AC bus are within a stable range. The general frequency fluctuation range is $\pm 0.5Hz$, and the voltage fluctuation range is $\pm 10\%$. Ensuring the stable operation of the microgrid is to ensure the system power balance, that is to say the power provided by the micro-source and the power required by the load remain realize stable so that the voltage and frequency at the AC bus will remain stable. The operation mode of the AC microgrid is divided into grid-connected operation and off-grid operation. When connected to the grid, the AC bus is connected to the distribution network through the circuit breaker. The voltage and frequency at the AC BUS are controlled by the distribution network. When off-grid operation, the circuit breaker of the AC bus is disconnected, and the voltage and frequency at the AC BUS are regulated by the respective micro-sources in the micro-grid. When the microgrid is switched from the grid-connected operation

mode to the off-grid operation mode, the circuit breaker at the AC BUS is disconnected and the AC microgrid is operated in the off-grid mode. When the microgrid is switched from the off-grid operation mode to the grid-connected operation mode, the voltage and frequency at the AC BUS need to be adjusted to be consistent with the distribution network, so that the circuit breaker can be closed to operate in the grid-connected operation mode. The simplified structure of the AC microgrid is shown in Fig. 1. The n micro-sources are respectively connected to the AC bus through the independent micro-source converter. The output power of the micro-source 1 is $[v_{a1} \quad v_{b1} \quad v_{c1}]$ and $[i_{a1} \quad i_{b1} \quad i_{c1}]$, the line impedance is Z_1, and so on. The output power of n -th micro-source is $[v_{an} \quad v_{bn} \quad v_{cn}]$ and $[i_{an} \quad i_{bn} \quad i_{cn}]$, the line impedance is Z_n. Assume that the output voltage of the distributed generation unit is $[v_a \quad v_b \quad v_c]$, and the output current is $[i_a \quad i_b \quad i_c]$, so the output power of the distributed generation unit is described as:

$$S = P + jQ = v_a i_a + v_b i_b + v_c i_c \tag{1}$$

Eq. (1) is the power calculation method of the distributed generation unit in the stationary coordinate system, but this calculation method is more complicated, the output voltage and the output current are both sinusoidal functions, and there is an angular difference. Therefore, the active power and reactive power of the distributed power generation unit are generally calculated in a rotating coordinate system. The power calculation of the three-phase micro-source converter in the rotating coordinate system requires the following steps:

1) Voltage and current parameters are converted to two-phase stationary coordinate system.

$$\begin{bmatrix} v_\alpha \\ v_\beta \\ v_0 \end{bmatrix} = \begin{bmatrix} 1 & -\frac{1}{2} & -\frac{1}{2} \\ 0 & \frac{\sqrt{3}}{2} & -\frac{\sqrt{3}}{2} \\ 1 & 1 & 1 \end{bmatrix} \begin{bmatrix} v_a \\ v_b \\ v_c \end{bmatrix} \tag{2}$$

$$\begin{bmatrix} i_\alpha \\ i_\beta \\ i_0 \end{bmatrix} = \begin{bmatrix} 1 & -\frac{1}{2} & -\frac{1}{2} \\ 0 & \frac{\sqrt{3}}{2} & -\frac{\sqrt{3}}{2} \\ 1 & 1 & 1 \end{bmatrix} \begin{bmatrix} i_a \\ i_b \\ i_c \end{bmatrix} \tag{3}$$

2) Voltage and current parameters are converted to two-phase rotating coordinate system

$$\begin{bmatrix} v_d \\ v_q \end{bmatrix} = \begin{bmatrix} \cos\theta & \sin\theta \\ -\sin\theta & \cos\theta \end{bmatrix} \begin{bmatrix} v_\alpha \\ v_\beta \end{bmatrix} \tag{4}$$

$$\begin{bmatrix} i_d \\ i_q \end{bmatrix} = \begin{bmatrix} \cos\theta & \sin\theta \\ -\sin\theta & \cos\theta \end{bmatrix} \begin{bmatrix} i_\alpha \\ i_\beta \end{bmatrix} \tag{5}$$

After the above transformations, the output apparent power of the distributed generation unit can be expressed as:

$$S = P + jQ = \frac{3}{2}\left(v_d i_d + v_q i_q\right) + j\frac{3}{2}\left(v_q i_d - v_d i_q\right) \tag{6}$$

There are two types of microgrid operation modes, one is the grid-connected operation mode and the other is the off-grid operation mode. In the off-grid operation mode, since the microgrid is not connected to the main grid through the connector, the voltage and frequency at the AC bus are regulated by the micro-sources in the micro-grid. Generally, the virtual impedance-based droop control strategy is used to achieve reactive power sharing and voltage control.

In the grid-connected mode, the voltage and frequency at the AC bus are regulated by the main grid, which is equivalent to the master-slave control. Each micro-source in the micro-grid uses PQ control to provide energy to the main grid and simultaneously supplies power to the local load.

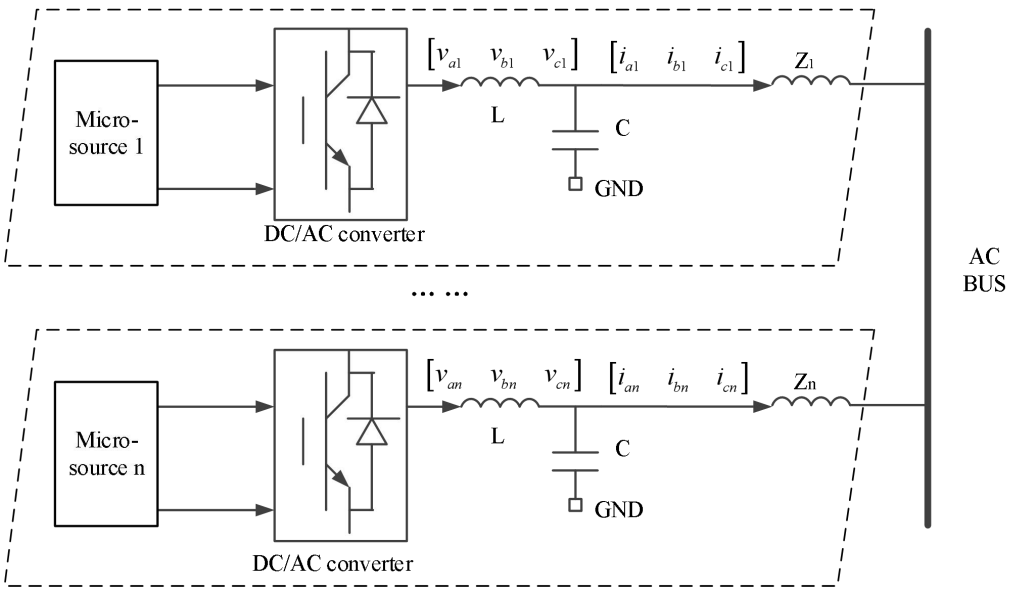

Fig. 1 Simplified architecture of AC microgrid.

Since the micro-sources in the micro-grid adopt droop control in the off-grid operation mode, the output voltage and frequency cannot be consistent with the main grid. When they are directly incorporated into the main grid without taking measures, the voltage, frequency and phase deviation will have a specific impact on each micro-source in the micro-grid, which will affect the stability of the micro-grid. Therefore, switching from the off-grid operation mode to the grid-connected operation mode requires a suitable off-grid switching strategy to make the microgrid smoothly transition from the grid.

III. Design of Microgrid Phase-locked Loop

Generally, the grid-connected synchronous control strategy needs to achieve three control objectives, that is to say to adjust the voltage deviation, frequency deviation and phase deviation between the microgrid and the main grid. After it reaches the consistent or very small range, close the line connector and realize grid-connected operation of microgrid. The phase-locked loop is an important link to realize the grid-connected operation of the micro-grid. It can provide the voltage, frequency and phase signals of the main power grid [21]. The structural diagram of a three-phase phase-locked loop based on a synchronous reference coordinate system is shown in Fig. 2.

The three-phase voltage of the main power grid obtain the grid voltage amplitude through rotational transformation, then it is controlled by the PI regulator to make it to 0. Then, the angular frequency of the grid voltage can be obtained, and the phase of the grid voltage can be obtained by integrating the grid voltage angular frequency. The grid voltage angular frequency is divided to get the frequency of the grid voltage. Therefore, the three-phase phase-locked loop based on the synchronous rotating coordinate system can obtain three key parameters required for grid-connected control: voltage, frequency and phase relationship.

As shown in Fig. 3, when carrying out the rotating transformation, the angle difference between the d axis and α axis is $\tilde{\theta}$. Then Eq. (7) and (8) are used to express the mathematical relationship between the grid voltage signal in the stationary coordinate system and the synchronous rotating coordinate system.

$$\begin{cases} v_\alpha = V\cos\theta \\ v_\beta = V\sin\theta \end{cases} \tag{7}$$

$$\begin{cases} v_d = V\cos\left(\theta-\tilde{\theta}\right) \\ v_q = V\sin\left(\theta-\tilde{\theta}\right) \end{cases} \tag{8}$$

When θ is close to $\tilde{\theta}$ nearly, there is $\sin\left(\theta-\tilde{\theta}\right)\approx\left(\theta-\tilde{\theta}\right)$ in Eq (9). So by adjusting v_q to be equal to zero, the phase angle parameter of the grid voltage can be obtained. However, when the grid voltage contains a large number of harmonics, the above-mentioned phase-locked loop method will have certain defects, which will result in a decrease in the accuracy of the phase-locked loop and an abnormality in the voltage, frequency and phase extraction of the grid [22]. Assume that in the distorted state, the grid voltage signal can be expressed as:

$$\begin{cases} v_a = V\sin\theta \\ v_b = (1+\chi)V\sin\left(\theta-\dfrac{2\pi}{3}\right) \\ v_c = (1+\lambda)V\sin\left(\theta-\dfrac{2\pi}{3}\right) \end{cases} \tag{9}$$

After transformation through the stationary coordinate system, the grid voltage signal can be described as:

$$\begin{cases} v_\alpha = V\sin\theta + V\left[\dfrac{\chi+\lambda}{6}\sin\theta - \dfrac{\chi-\lambda}{2\sqrt{3}}\cos\theta\right] \\ v_\beta = -V\sin\theta + V\left[\sin\theta - \dfrac{\chi+\lambda}{6}\cos\theta\right] \end{cases} \tag{10}$$

Rotate and simplify Eq. (10) to obtain:

$$v_q = V\sin\left(\theta-\tilde{\theta}\right) - V\left[\frac{\chi+\lambda}{6}\sin\left(\theta+\tilde{\theta}\right) + \frac{\chi-\lambda}{2\sqrt{3}}\cos\left(\theta+\tilde{\theta}\right)\right] \tag{11}$$

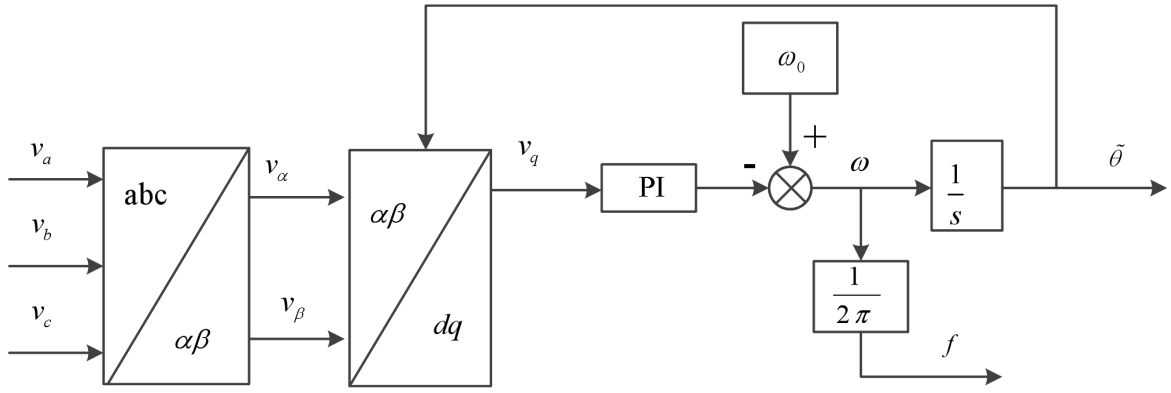

Fig. 2 Structure of three phase locked loop based on synchronous reference frame.

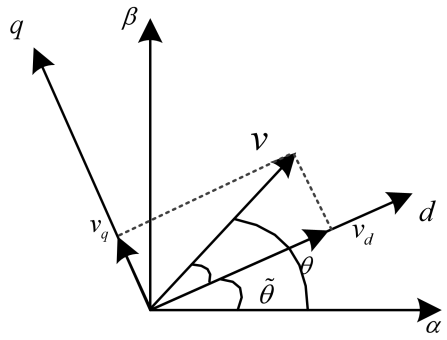

Fig. 3 Grid-connected pre-synchronous control.

By comparing Eq (8) and (11), in the case of grid distortion, it is not possible to track the grid voltage phase by adjusting v_q to zero because there is a disturbance term in the phase [23]. So a new three-phase phase-locked loop structure is adopted to solve the problem of phase-locking inaccuracy in the case of grid voltage distortion. For an asymmetric three-phase system, it can be converted into the sum of symmetric positive sequence, negative sequence and zero sequence vector [24], so the grid voltage signal in the distorted state can be expressed as:

$$\begin{cases} v_a = V^+ \sin\theta + V^- \sin\left(-\theta+\phi\right) + V^0 \sin\left(\theta+\varphi\right) \\ v_b = V^+ \sin\left(\theta-\dfrac{2\pi}{3}\right) + V^- \sin\left(-\theta-\dfrac{2\pi}{3}+\phi\right) + V^0 \sin\left(\theta+\varphi\right) \\ v_c = V^+ \sin\left(\theta+\dfrac{2\pi}{3}\right) + V^- \sin\left(-\theta+\dfrac{2\pi}{3}+\phi\right) + V^0 \sin\left(\theta+\varphi\right) \end{cases} \tag{12}$$

Perform the positive sequence Park rotation transformation on Eq. (12) to obtian:

$$\begin{cases} v_{dp} = V^+ \cos\left(\theta-\tilde{\theta}\right) + V^- \cos\left(-\theta-\tilde{\theta}+\phi\right) \\ v_{qp} = V^+ \sin\left(\theta-\tilde{\theta}\right) + V^- \sin\left(-\theta-\tilde{\theta}+\phi\right) \end{cases} \tag{13}$$

Perform the negative sequence Park rotation transformation on Eq. (12) to get:

$$\begin{cases} v_{dn} = V^+ \cos\left(\theta+\tilde{\theta}\right) + V^- \cos\left(-\theta+\tilde{\theta}+\phi\right) \\ v_{qn} = V^+ \sin\left(\theta+\tilde{\theta}\right) + V^- \sin\left(-\theta+\tilde{\theta}+\phi\right) \end{cases} \tag{14}$$

It can be seen from Eq. (13) that when locked to the grid voltage phase angle, there is a double-frequency disturbance signal of the v_{qp} negative sequence voltage [25]. It can be seen from Eq. (14) that when locked to the grid voltage phase angle, there is a double frequency disturbance signal of the v_{qn} positive sequence voltage. The double frequency signal can be expressed as:

$$\begin{cases} v_{dp} = V^+ + V^- \cos\left(-2\tilde{\theta}+\phi\right) \\ v_{qp} = 0 + V^- \sin\left(-2\tilde{\theta}+\phi\right) \end{cases} \tag{15}$$

$$\begin{cases} v_{dn} = V^+ \cos\left(2\tilde{\theta}\right) + V^- \cos\left(\phi\right) \\ v_{qn} = V^+ \sin\left(2\tilde{\theta}\right) + V^- \sin\left(\phi\right) \end{cases} \tag{16}$$

To this end, this paper uses a double decoupling coordinate transformation to eliminate the double frequency disturbance signal at the phase tracking time. The double frequency disturbance in Eq. (15) can be expressed as:

$$\begin{bmatrix} V^- \cos\left(-2\tilde{\theta}+\phi\right) \\ V^- \sin\left(-2\tilde{\theta}+\phi\right) \end{bmatrix} = \begin{bmatrix} \cos\left(-2\tilde{\theta}\right) & -\sin\left(-2\tilde{\theta}\right) \\ \sin\left(-2\tilde{\theta}\right) & \cos\left(-2\tilde{\theta}\right) \end{bmatrix} \begin{bmatrix} V^- \cos\left(\phi\right) \\ V^- \sin\left(\phi\right) \end{bmatrix} \tag{17}$$

where, $V^- \cos\left(\phi\right)$ and $V^- \sin\left(\phi\right)$ are the DC components in the negative sequence signal.

The double frequency perturbation in Eq. (16) can be expressed as [26]:

$$\begin{bmatrix} V^+ \cos\left(2\tilde{\theta}\right) \\ V^+ \sin\left(2\tilde{\theta}\right) \end{bmatrix} = \begin{bmatrix} \cos\left(-2\tilde{\theta}\right) & \sin\left(-2\tilde{\theta}\right) \\ -\sin\left(-2\tilde{\theta}\right) & \cos\left(-2\tilde{\theta}\right) \end{bmatrix} \begin{bmatrix} V^+ \\ 0 \end{bmatrix} \tag{18}$$

where, V^+ and zero is the DC component of the positive sequence signal.

By extracting the DC component in the negative sequence signal, the double frequency disturbance in the positive sequence signal is obtained by the double frequency park transform. Then it is superimposed on the positive sequence signal to eliminate the double frequency signal. The specific phase locked loop structure is shown in Fig. 4.

The input signal is $\begin{bmatrix} v_a & v_b & v_c \end{bmatrix}$ as shown in the Eq. (12). $\begin{bmatrix} v_\alpha & v_\beta \end{bmatrix}$ is obtained by the Clark transform, and it is performed through positive-sequence park transform to obtain the grid voltage signal shown in Eq. (13). The grid voltage signal shown in Eq. (14) is obtained by performing negative sequence park conversion.

For the negative sequence signal in the Eq. (16) simplified by Eq. (14), the DC signal is extracted by the low-pass filter, and the negative-order DC signal is performed the double-frequency park transformation by Eq. (17) to obtain the double-frequency disturbance in the positive sequence signal. Then the quantity is superimposed on the positive sequence signal to obtain the signal $v_q = V\left(\theta-\tilde{\theta}\right)$. Bu using PI adjustment, the grid voltage frequency signal is obtained, then the frequency signal is integrated to obtain the grid voltage phase signal $\tilde{\theta}$. According to Fig. 4, the open-loop transfer function of the phase-locked loop can be written as:

$$\phi_o(s) = V\left(k_{p\_pll} + \frac{k_{i\_pll}}{s}\right)\frac{1}{s} = V\frac{k_{p\_pll}s + k_{i\_pll}}{s^2} \tag{19}$$

where: $k_p + \dfrac{k_i}{s}$ is the transfer function of the PI controller.

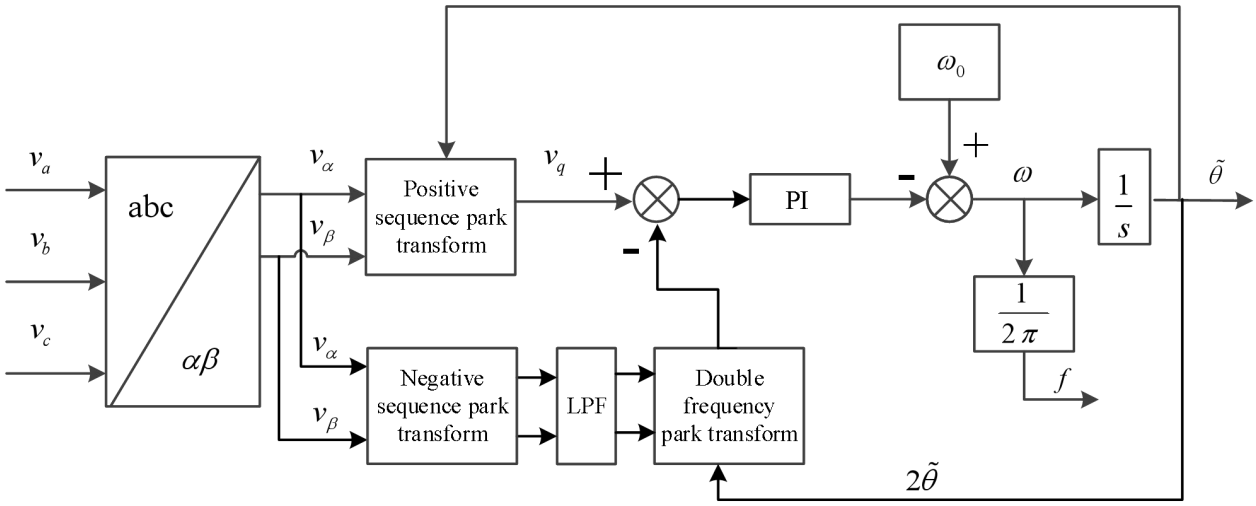

Fig. 4 Structure of phase locked loop based on double decoupling.

Based on the open-loop transfer function, the closed-loop transfer function of the phase-locked loop can be written as:

$$\phi_C(s)=\frac{\phi_o(s)}{1+\phi_o(s)}=\frac{V\left(k_{p\_pll}s+k_{i\_pll}\right)}{s^2+V\left(k_{p\_pll}s+k_{i\_pll}\right)} \tag{20}$$

According to the second-order eigenvalue equation of the control system [27], obtain:

$$s^2+2\xi\omega_0 s+\omega_0^2=0 \tag{21}$$

According to the optimal parameters of the second-order control system, there are:

$$\begin{cases} k_p=2\xi\omega_0/V \\ k_i=\omega_0^2/V \end{cases} \tag{22}$$

where, ξ is 0.707, and ω_0 314 rad/sec. The step response curve of the closed-loop transfer function of the phase-locked loop is shown in Fig. 5. According to the step response curve, the dynamic characteristics of the controller are well, reaching steady state at about 0.025s, which is equivalent to a cycle adjustment time of the grid. The overshoot is about 20%, which is also within a reasonable range.

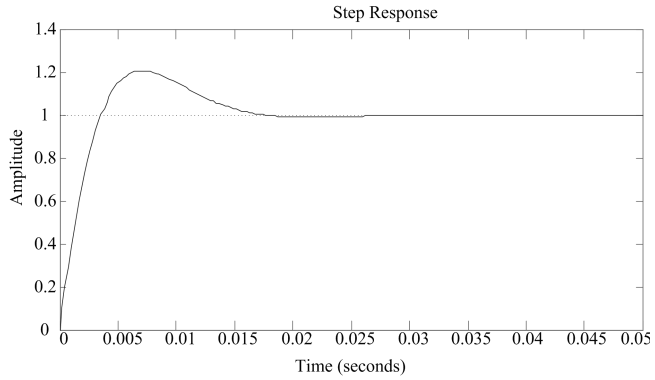

Fig. 5 Step response curve of PLL.

A low-pass filter for extracting a DC signal is generally classified into the first-order low-pass filter and the second-order low-pass filter. The first-order low-pass filter is simple to implement but the high-frequency signal is poorly eliminated. The second-order low-pass filter has a strong ability to filter out high-frequency signals, but the implementation is more complicated [28]. In this paper, a first-order low-pass filter is selected as the filter for extracting the DC component of the negative sequence signal, which can be expressed as:

$$H_L=\frac{\omega_c}{s+\omega_c} \tag{23}$$

Since the grid voltage signal is 50 Hz, the frequency of the double-frequency disturbance signal is 628 rad/sec, and the cutoff frequency of the filter is 1/10 of the high-frequency signal, so the cutoff frequency $\omega_c=62.8 rad/\sec$.

IV. Switching Strategy between On-grid and Off-grid Connection

The off-grid operation mode and the grid-connected operation mode of the microgrid adopt different control strategies, which leads to the inconsistency of the voltage, frequency and phase of the microgrid and the main grid. In order to realize the microgrid switching from the off-grid operation mode to the grid-connected operation mode, the off-grid and grid-connected switching controller is necessary. The improved droop controller can realize the secondary regulation of voltage and frequency, which can control the difference between the micro-grid AC bus and the mains AC bus voltage, frequency and phase, and improve the stability of the microgrid grid-connected operation. The microgrid off-grid and grid-connected control strategy is studied. By adopting the parameter matching of droop control and PQ control, a smooth transition switching from off-grid to grid-connected is realized [29]. The micro-grid smooth switching strategy based on fuzzy control is adopted, and the

fast phase tracking adjustment is realized by the fuzzy phase controller [20]. The grid-connected operation strategy based on the droop controller was proposed, which adopts voltage and frequency secondary regulation control to realize fast switching from off-grid to grid-connected [31]. Based on the small-signal model, the stability analysis of micro-grid switching to island operation was analyzed and a simplified micro-grid control model was proposed [32]. The control method of smooth switching of microgrid from the perspective of voltage and frequency was discussed [33]. Based on the mechanism of the surge voltage caused by the grid-connected of the micro-grid, a grid-connected pre-synchronization controller based on voltage, phase and frequency adjustment was constructed, which can realize the fast and smooth switching of the microgrid from off-grid to grid-connected and ensure the stability of the grid connection instantaneous system.

A. Analysis on Impulse Voltage at the Grid Connection Moment

The grid-connected pre-synchronization controller of the micro-grid is one of the main controllers for the stable operation of the micro-grid, which can effectively reduce the impact of the main grid on the micro-grid at the grid-connecting time [34]. Assume that before the grid-connected, the voltage at the AC bus and the main grid are described as:

$$v_m = V_m \sin\left(\omega_m t + \theta_m\right) \tag{24}$$

$$v_g = V_g \sin\left(\omega_g t + \theta_g\right) \tag{25}$$

Eq. (24) is the micro-grid AC bus voltage and m is the abbreviation of micro grid. Eq. (25) is the main grid AC bus voltage and g is the abbreviation of grid. At the moment of grid-connected, the difference between the AC voltage of the main grid and the microgrid is calculated by:

$$\Delta v = v_g - v_m = V_g \sin\left(\omega_g t + \theta_g\right) - V_m \sin\left(\omega_m t + \theta_m\right) \tag{26}$$

It can be seen form Eq. (26) that the voltage difference at the moment of grid-connected is related to the voltage amplitude, phase and frequency. Therefore, the comparative analysis of the impact of the three factors on the impact voltage is described as follows.

1) Assume that the voltage amplitude, frequency and phase relationship of the microgrid are exactly the same as the voltage amplitude, frequency and phase relationship of the main grid, that is $\Delta v = 0$. At the time of grid-connected, there is no surge voltage, which belongs to smooth switching grid-connected. However, such grid-connected conditions are difficult to implement without the presence of a grid-connected pre-synchronization controller, and the probability is almost zero. But this is the main purpose of the grid-connected pre-synchronization controller design.

2) Assume that the voltage and frequency are the consistent and the phases are different, so Eq. (26) can be rewritten as:

$$\Delta v = v_g - v_m = 2V \sin\left(\frac{\theta_g - \theta_m}{2}\right)\cos\left(\text{wt} + \frac{\theta_g + \theta_m}{2}\right) \tag{27}$$

At the moment, the surge voltage is related to phase, the surge voltage is maximum when the phase deviation is 180° , and the maximum surge voltage is $2V$.

3) Assuming that the amplitude and phase are consistent, but the frequencies are inconsistent, Eq. (26) can be rewritten as:

$$\Delta v = v_g - v_m = 2V \sin\left(\frac{\omega_g - \omega_m}{2}t\right)\cos\left(\frac{\omega_g + \omega_m}{2}t + \theta\right) \tag{28}$$

At this time, the surge voltage is related to the frequency, and the grid-connected surge voltage is minimized at the zero-crossing point.

4) Assuming that the frequency and phase are the consistent, but the amplitudes are inconsistent, then Eq. (26) can be rewritten as:

$$\Delta v = v_g - v_m = \left(V_g - V_m\right)\sin\left(\omega t + \theta\right) \tag{29}$$

At this time, the surge voltage is related to the amplitude, and the maximum surge voltage is $V_g - V_m$. Depending on the magnitude and phase deviation of v_g and v_m at the grid-connected time, different voltage differences will occur. In the worst case, when their amplitudes are the same, but the phases are 180° out of phase, the voltage deviation at this time is the largest. Therefore, the phase deviation has a very large influence on the voltage deviation at the time of grid-connected.

B. Design of Grid-connected Pre-synchronization Controller

In the process of switching the microgrid from the off-grid mode to the grid-connected mode, when the voltage, frequency and phase of micro-grid are greatly deviated from the main grid, since the transient impact voltage is too large, which can cause a destructive impact on the power equipment of the micro-grid, even make the microgrid collapse, it is necessary to design a grid-connected synchronous controller to reduce the surge voltage at the moment of grid-connected [35]. The traditional grid-connected synchronous controller is generally implemented based on the droop control strategy, mainly through the secondary adjustment of voltage and frequency, so that the output voltage and frequency of the drooping controller and the grid voltage and frequency are kept in a small interval. Then the grid-connected switch is started and the microgrid enters the grid-connected operation mode. However, considering that the phase deviation has a great influence on the instantaneous surge voltage of the grid-connected, it is necessary to add a phase adjuster based on the voltage and frequency secondary control so as to

control the operation phase angle of the microgrid and make it keep pace or have small deviation with the phase angle of the grid. As shown in Fig. 6, it is assumed that at a certain moment, the corresponding voltage and frequency at the AC bus of the microgrid are V_1 and f_1 respectively, and the voltage and frequency of the grid are V0 and f0 respectively. When the grid-connected pre-synchronization controller is started, the active droop curve and the reactive drooping curve respond up. At the same time, the voltage and frequency of the micro-grid AC bus also run at V_0 and f_0. when the grid-connected pre-synchronization controller ends, the microgrid is switched from the off-grid mode to the grid-connected mode.

Through the voltage and frequency secondary regulation under the droop control, the voltage and frequency of the microgrid can be synchronized with the main grid, and the deviations of the secondary voltage regulation and the secondary frequency regulation are $f_g = f_L + f_{err} = f_n - m(P - P_n) + f_{err}$ and $f_g = f_L + f_{err} = f_n - m(P - P_n) + f_{err}$, respectively, which can be calculated by:

$$f_{\text{ref}} = f_n - m(P - P_n) + f_{err} \tag{30}$$

$$V_{ref} = V_n - n(Q - Q_n) + V_{err} \tag{31}$$

Secondary voltage and frequency regulation is typically by introducing a voltage and frequency PI regulator to achieve synchronize with the grid voltage and frequency. The reference value of the secondary regulator is provided by the PLL and the feedback signal is provided by the droop controller. For the target of phase synchronization, an additional phase adjuster is also required. At the same time, in order to achieve fast synchronization of voltage, frequency and phase, the drooping controller are introduced to control the output voltage, frequency and phase. Feed forward is adopted in the voltage, frequency and phase regulator so as to accelerate the dynamic response of the grid-connected pre-synchronization controller. Therefore the equations for voltage, frequency and phase regulators are shown in Eq. (32)-(34).

$$V_{ref} = (V_g - V)(k_p + k_i / s) + V \tag{32}$$

$$f_{ref} = (f_g - f)(k_p + k_i / s) + f \tag{33}$$

$$\theta_{ref} = (\theta_g - \theta)(k_p + k_i / s) + \theta \tag{34}$$

Fig. 7 is a block diagram of the grid-connected pre-synchronization controller, where the phase-locked loop provides the grid voltage, frequency and phase detection values V_g, f_g and θ_g, and the droop controller provides the voltage and frequency feedback signals V and f. The phase feedback signal is integrated by the frequency reference value, that is $\theta = 2\pi f_{ref} / s$. The specific implementation of the grid-connected synchronous controller is described as follows. Based on the deviation of the grid voltage and the droop control feedback voltage after the synchronous start of the grid-connected, the voltage regulation can be realized by the PI controller, and the fast tracking of voltage can be realized through the feed-forward of the voltage V. The the integral link in the PI controller can reduce the steady-state error of the system as much as possible, improve the accuracy of the voltage regulator, and reduce the high-frequency interference signal. The principle of the frequency regulator and phase regulator is consistent with the principle of the voltage regulator. The voltage, frequency and phase signals obtained by the grid-connected pre-synchronization controller are applied to the voltage-current controller to adjust the output voltage of the micro-grid converter. The grid-connected detector detects the actual value of the voltage, frequency and phase at the AC bus of the microgrid, and compares it with the actual output values of the main grid voltage, frequency and phase by the PLL. If the deviation is within the tolerable range, the grid-connected contactor starts. At the same time, all the micro-source converters in the micro-grid are switched from droop control to PQ control, and the micro-grid is connected to the grid-connected operation mode. The feed forward-based phase PI regulator, although its dynamic response speed is already fast, but it is located behind the frequency regulator, so its response time still needs to be improved.

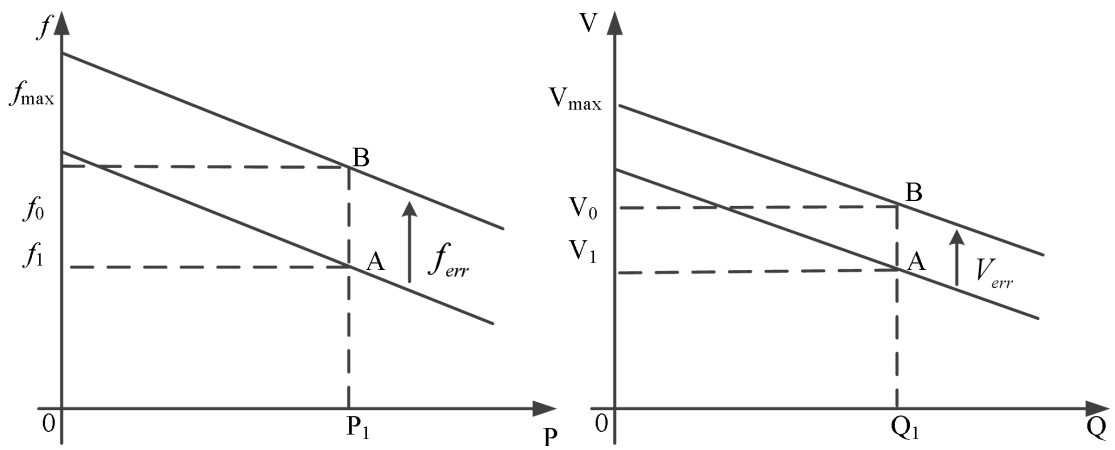

Fig. 6 Secondary regulation of voltage and frequency.

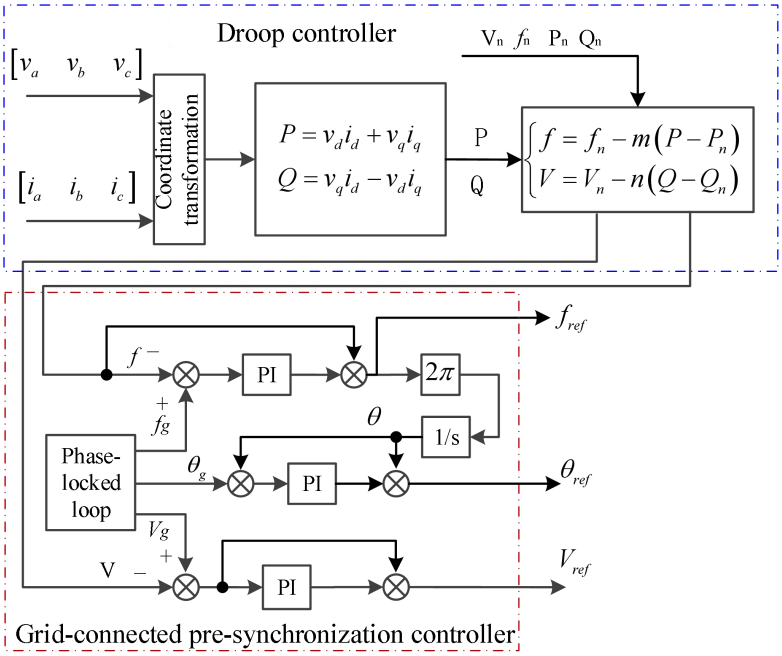

Fig. 7 Structure of on-grid synchronization controller.

In order to improve the time response of the phase adjuster and improve the output accuracy of the phase adjuster, this paper adopts a new phase adjuster with linear approximation to improve the feed forward link based on the traditional phase adjuster by introducing a time series increasing function. The phase reference value is quickly adjusted, and the accuracy of the sequence increasing function is also relatively high, which does not cause a large overshoot to produce a phase adjustment oscillation process. The new phase regulator structure is shown in Fig. 8.

In the new phase adjuster, the phase adjustment value is composed of two parts: one part is generated by the PI regulator, mainly to adjust the steady-state error of the phase and improve the accuracy of the phase tracking; the other part is generated by the feed forward link mainly through the time series function, which is used to improve the speed of phase tracking and speed up the adjustment time of the grid pre-synchronization controller. So the new phase adjustment strategy can be described as:

$$\theta_{ref} = \left(\theta_g - \theta\right)\left(k_p + k_i / s\right) + Kt\left(\theta_g - \theta\right) \qquad (35)$$

V. Division of the Off-Grid and On-Grid Operation Condition of the Microgrid

Generally, the division of the grid-connected operating conditions of the AC microgrid is based on the change of the voltage and frequency at the AC bus. The reference frequency of the AC microgrid is 50 Hz and the reference voltage is 220V. Because in the off-grid operation state, each micro-source converter in the system adopts the droop control strategy, the AC voltage and frequency are dynamically changed. Generally, the voltage fluctuation range is 198V~242V and the frequency operation range is 49.5Hz~50.5Hz, which is the normal threshold for the operation of the microgrid. When the voltage and frequency of the microgrid drop to between 187V and 198V and between 49Hz and 49.5Hz, it is considered to be overloaded. At this time, it is necessary to access the distribution network.

When the voltage and frequency of the microgrid drop to between 242V and 253V and between 50.5Hz and 51Hz, it is considered to be a state of excess power generation, and it is necessary to access the distribution network. As shown in Fig. 9, the AC frequency mode can be divided into four zones. The interval I is in the range of 49.5 Hz to 50.5 Hz, which belongs to the normal working area. The interval II is between 50.5 Hz and 51 Hz, which belongs to the light load zone. The interval III is between 49 Hz and 49.5 Hz and belongs to the heavy load zone. The interval IV is a frequency exceeding 51 Hz or lower than 49 Hz and belongs to the working abnormal zone. The AC voltage mode can be divided four zones, which is shown in Fig. 10. The interval I is in the range of 198V~242V, which belongs to the normal working area. The interval II is between 242V and 253V and belongs to the light load zone. The interval III is between 187V and 198V and belongs to the heavy load zone. The interval IV is a voltage exceeding 253V or lower than 187V, which belongs to the working abnormal zone. By analyzing Fig. 9 and Fig. 10, the conditions for the microgrid to access the main grid can be clarified. When the microgrid runs to the II or III interval, the microgrid can conditionally decide whether to access the main grid. When the microgrid is operating in the IV interval, the microgrid must be connected to the main grid. When the microgrid is operating in the I interval, it is not recommended to access the main grid.

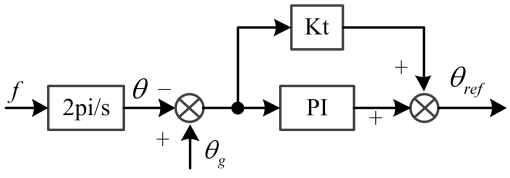

Fig. 8 The block diagram of phase regulator.

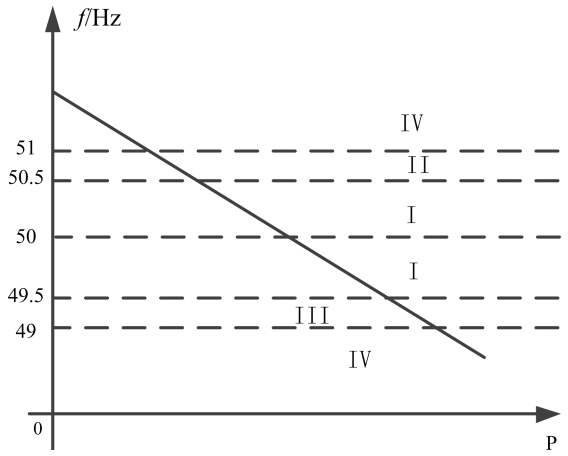

Fig. 9 Microgrid frequency operating range.

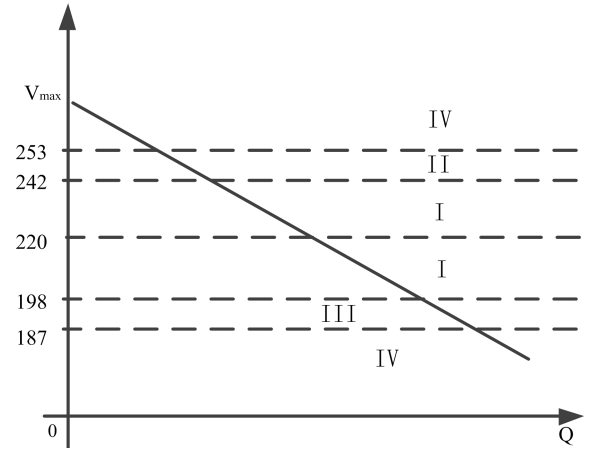

Fig. 10 Microgrid voltage operating range.

VI. Simulation Verification

The simulation verification is mainly for the proposed phase-locked loop design based on double decoupling transformation strategy and the smooth switching control strategy from the off-grid to grid-connected.

A. Simulation on Phase-locked Loop

The simulation waveform of the conventional phase-locked loop in the case of three-phase symmetry of the grid voltage is shown in Fig. 11. According to the phase waveform, the phase-locked loop can track the phase change of the grid voltage very well. Fig. 12 shows the grid voltage amplitude and frequency parameters extracted by the traditional phase-locked loop. According to the waveform, the phase-locked loop can not only track the phase change of the grid voltage, but also extract the amplitude and frequency of the grid voltage. According to the waveform, the voltage amplitude is 311V and the grid frequency is 50Hz.

Fig. 13 shows the phase waveform extracted by the grid voltage and phase-locked loop when the grid voltage is a three-phase asymmetric system. According to the waveform, the amplitude of the grid voltage has been severely distorted, and the phase waveform of the phase-locked loop output is also fluctuating, so the phase of the grid voltage cannot be accurately tracked. Fig. 14 shows the grid voltage amplitude and frequency data extracted by the traditional phase-locked loop in the case of severe grid voltage distortion. According to the waveform, the phase-locked loop can not only track the phase change of the grid voltage, but also the grid voltage amplitude and frequency data extracted by the traditional phase-locked loop are also oscillating. Through the above simulation, the phase-locking accuracy, amplitude extraction and frequency extraction of the traditional phase-locked loop cannot maintain high efficiency under the grid voltage distortion state. Fig. 15 shows the MATLAB simulation model of a new phase-locked loop structure with double decoupling. Based on the traditional phase-locked loop, the Q-axis double-frequency disturbance variable is extracted and eliminated by the double decoupling link so as to realize the tracking control of the PI regulator. When the grid voltage is a three-phase asymmetric system, the grid voltage and the phase waveform extracted by the new double decoupled phase-locked loop are shown in Fig. 16. According to the waveform in Fig. 16, although the amplitude of the grid voltage has been severely distorted, the phase waveform output of the phase-locked loop is still stable and has good tracking accuracy. It can be seen from the comparison simulation that when the grid voltage is severely distorted, the double decoupled phase-locked loop can eliminate the double-frequency disturbance contained in the Q-axis, thus improving the tracking accuracy of the phase-locked loop.

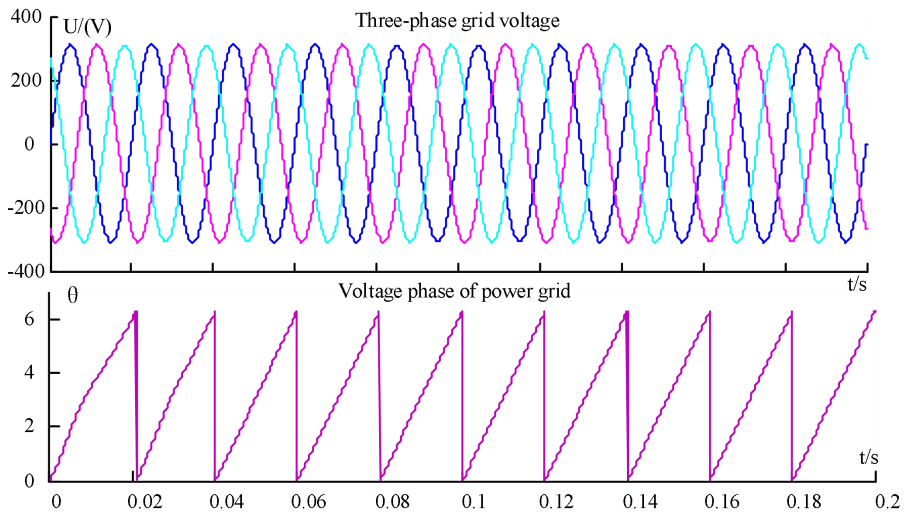

Fig. 11 The voltages and phase waves of traditional PLL.

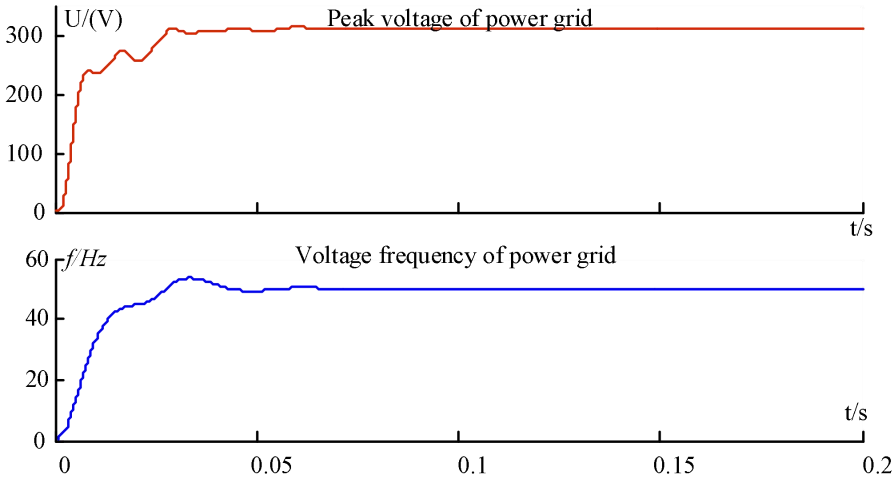

Fig. 12 The voltage amplitude and frequency waves of traditional PLL.

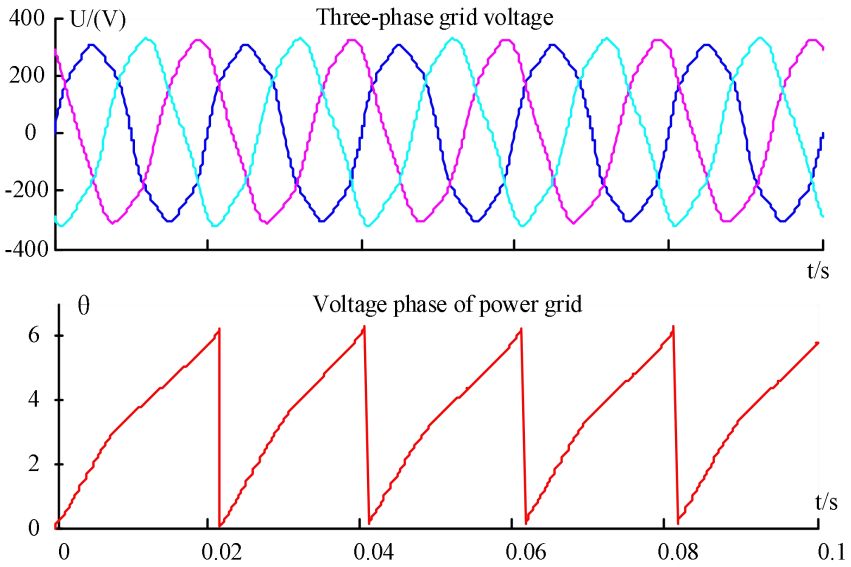

Fig. 13 The voltages and phase waves in distorted grid.

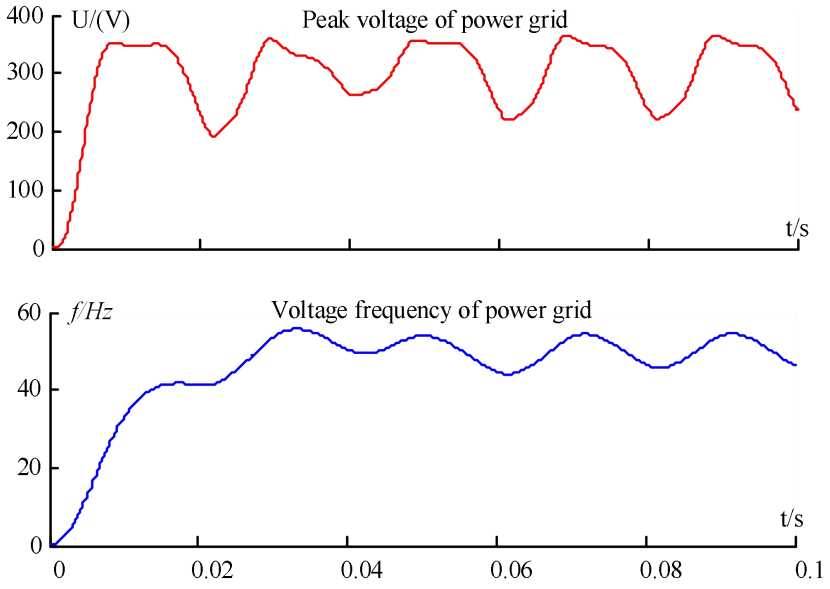

Fig. 14 The voltage amplitude and frequency waves in distorted grid.

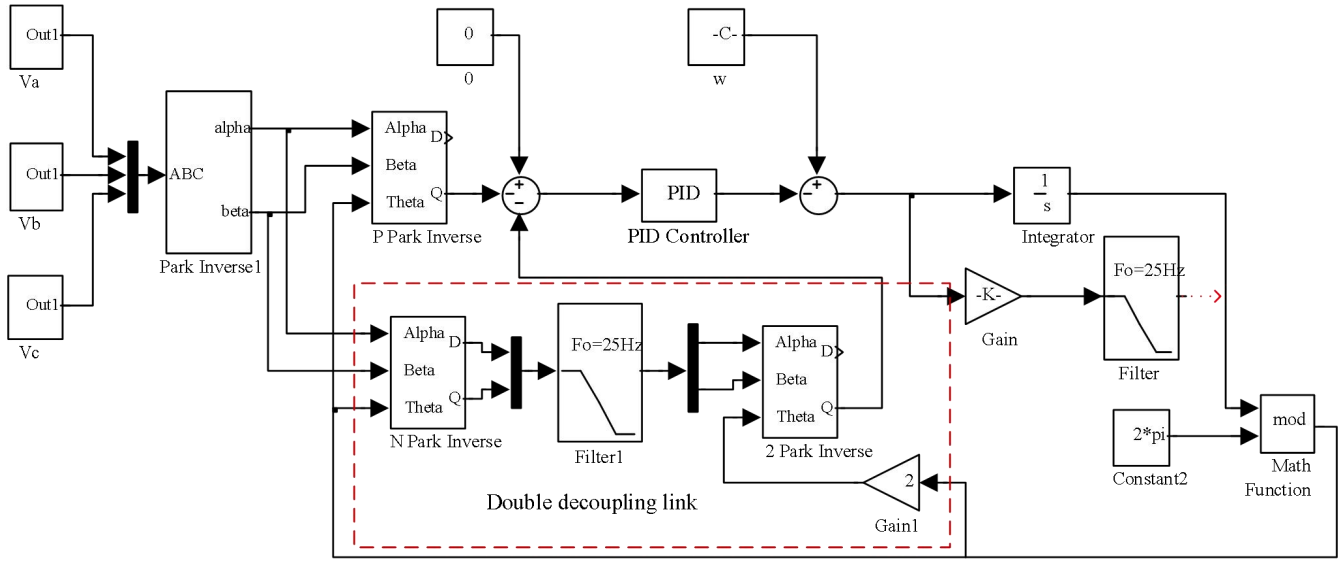

Fig. 15 The simulation model of new PLL.

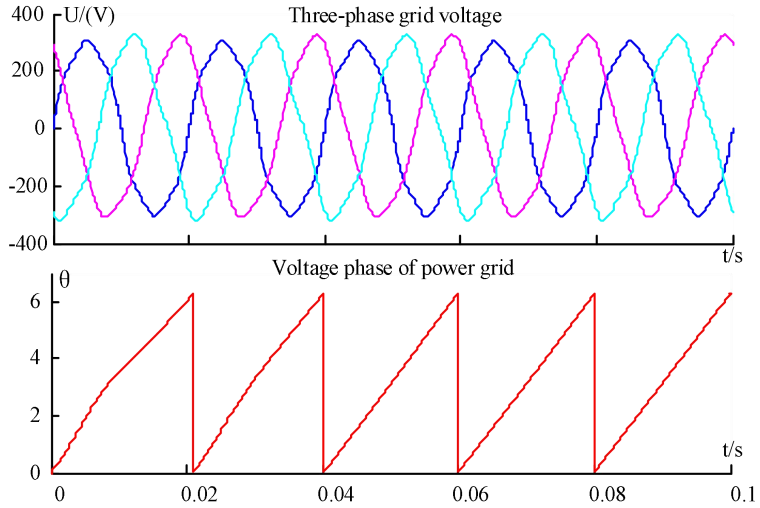

Fig. 16 The voltages and phase waves of novel PLL.

B. Simulation on On-grid and Off-grid Switching

The following simulation is carried out in MATLAB. The initial time of the microgrid is loaded with S1=7kW+j3.5kVar, and at 0.16s the new load S2=2kW+j0.5kVar is connected. The frequency waveform of the output voltage of the micro-source inverter is shown in Fig. 17. The voltage frequency is 49.65 Hz at S1 load. After switched into the S2 load at 0.16 s, the voltage frequency drops to 49.4 Hz. At this point, the microgrid operates in the heavy load zone. At the time of 0.2s, the grid-connected pre-synchronization controller is started, and the voltage frequency gradually rises, which will reach about 50 Hz at about 0.22 s, and wait for the grid-connected signal. The output voltage waveform of the micro-source inverter is shown in Fig. 18. The voltage is 216V under S1 load. After switched into the S2 load at time 0.16s, the voltage drops to 212V. Due to the low frequency, at the time of 0.2s, the grid-connected pre-synchronization controller is started, and the voltage frequency gradually rises, which will reach about 220VHz at about 0.22s, and wait for the grid-connected signal. The load power at the AC bus is shown in Fig. 19. At the time of 0.2s, the grid-connected pre-synchronization controller is started, and the voltage and frequency of the micro-grid AC bus change, so it can be seen that the load power starts to oscillate. At about 0.22 s, the load power also began to stabilize as the voltage and frequency returns to steady state. Based on the above simulation, it can be seen that the grid-connected pre-synchronization control can be realizing the effective adjustment of the AC bus voltage and frequency of the micro-grid, which is consistent with the grid voltage and frequency to achieve grid connection.

VII. Conclusion

The smooth switching control strategy of microgrid from off-grid to grid-connected was analyzed. The traditional phase-locked loop has poor accuracy in voltage phase, amplitude and frequency extraction under grid voltage distortion. Therefore, a double decoupled phase-locked loop structure is adopted to improve the accuracy of the phase-locked loop. At the same time, it analyzes the causes of the surge voltage at the time of the off-grid to grid-connected switching, and then a grid-connected pre-synchronization control strategy was proposed to reduce the impact on the microgrid at the moment of grid-connected. Finally, the proposed control strategy was verified by simulation experiments.

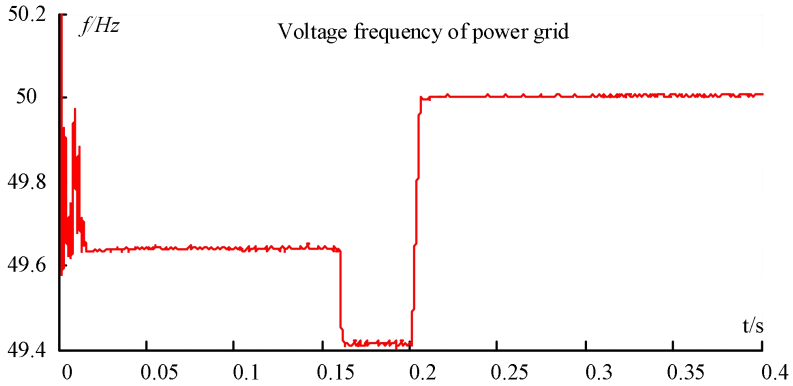

Fig. 17 The voltages waves of AC bus.

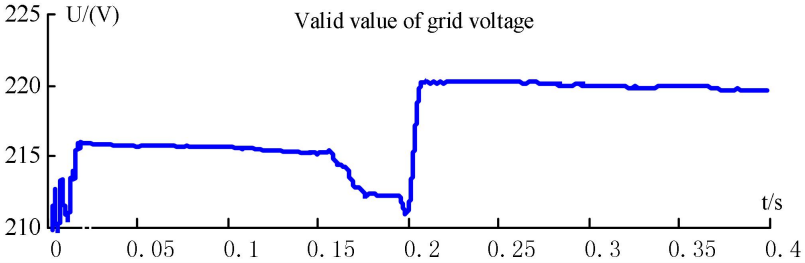

Fig. 18 The frequency waves of AC bus.

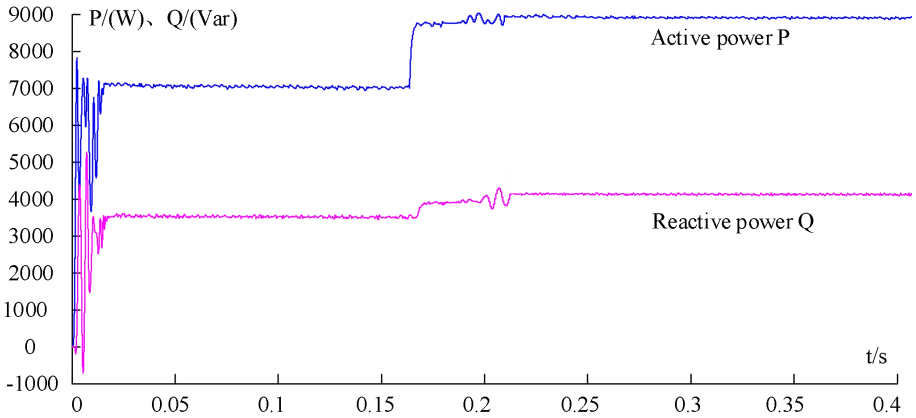

Fig. 19 The load power waves of load in AC bus.

REFERENCES

[1] J. W. Cao, K. Meng, J. Y. Wang, M. B. Yang, Z. Chen, W. Z. Li, and C. Lin, "An Energy Internet and Energy Routers," *Scientia Sinica (Informationis)*, vol. 44, no. 6, pp. 714-727, 2014.

[2] S. Tian, W. Luan, D. Zhang, C. Liang, and Y. Sun, "Technical Forms and Key Technologies on Energy Internet," *Proceedings of the Chinese Society of Electrical Engineering*, vol. 35, no. 14, pp. 3482-3494, 2015.

[3] J. L. Li, L. T. Tian, and X. K. Lai, "Outlook of Electrical Energy Storage Technologies Under Ender Internet Background," *Automation of Electric Power Systems*, vol. 23, pp. 15-25, 2015.

[4] W. H. Cui, J. S. Wang, and Y. Y. Chen, "Equivalent Circuit Model of Lead-acid Battery in Energy Storage Power Station and its State-of-Charge Estimation Based on Extended Kalman Filtering Method," *Engineering Letters*, vol. 26, no. 4, pp. 504-517, 2018.

[5] H. Morais, Kádár Péter, P. Faria, Z. A. Vale, and H. M. Khodr, " Optimal Scheduling of a Renewable Microgrid in an Isolated Load Area Using Mixed-integer Linear Programming," *Renewable Energy*, vol. 35, no. 1, pp. 151-156, 2010.

[6] X. Z. Yang, S. U. Jian-Hui, M. Ding, and D. U. Yan, "Research on Frequency Control for Microgrid in Islanded Operation," *Power system technology*, vol. 34, no. 1, pp. 164-168, 2010.

[7] M. Ding, L. G. Tian, H. Pan, X. S. Zhang, and J. H. Zhou, "Research on Control Strategy of Hybrid AC/DC Microgrid," *Power System Protection and System*. vol.43, no. 9, pp. 1-8, 2015.

[8] Y. C. Xue, N. L. Tai, L. Q. Liu, X. W. Yang, N. Jin, and N. Xiong, "Co-operation Control Strategies for Islanded Microgrids," *Electric Power*, vol. 42, no. 7, pp. 36-40, 2009.

[9] W. Liu, "A Study of Master-slave Control Strategy in Isolated Microgrid ," *Journal of WuYi University*, vol. 25, no. 3, pp. 56-60, 2011.

[10] Y. S. Chen, P. Yang, Z. J. Zeng, and J. J. Peng, "Planning of Distributed Energy Resources for Distribution Network Considering Dispatchable Region of Microgrids," *Automation of Electric Power Systems*, vol. 43, no. 3, pp. 83-91, 2019.

[11] J. J. Jiang, and R. Ju, "Summary of Microgrid Control Technology," *Advanced Materials Research*, vol. 1070-1072, pp. 1326-1334, 2015.

[12] X. Zhu, J. Liu, Y. Liu, Y. Xiang, and H. Tian, "Study of Microgrid Control Strategy Contained Unbalanced Load Based on Sliding-mode Variable Structure," *Power System Protection and Control*, vol. 43, no. 6, pp. 25-32, 2015.

[13] P. M. S. Carvalho, P. F. Correia, and L. A. F. M. Ferreira, "Distributed Reactive Power Generation Control for Voltage Rise Mitigation in Distribution Networks," *IEEE Transactions on Power Systems*, vol. 23, no. 2, pp. 766-772, 2008.

[14] A. I. Xin, J. Peng, and Y. Y. Sun, "An Enhanced Reactive Sharing Control Strategy of Microgrid," *Power System Protection and System*, vol. 41, no. 7, pp. 147-155, 2013.

[15] F. C. Lu, and Y. Y. Hsu, "Fuzzy Dynamic Programming Approach to Reactive Power/Voltage Control in a Distribution Substation," *IEEE Transactions on Power Systems*,vol.12, no. 2, pp. 681-688, 1997.

[16] F. C. Lu, and Y. Y. Hsu, "Reactive Power/Voltage Control in a Distribution Substation Using Dynamic Programming," *Generation, Transmission and Distribution, IET Proceedings-*, vol. 142, no. 6, pp. 639-645, 1995.
[17] B. Lu, and N. Yi, "A Self-approximate-optimal Distributed Reactive Power and Voltage Control Strategy for Microgrid in Island Mode," *Automation of Electric Power Systems*, vol. 38, no. 9, pp. 218-225, 2014.
[18] L. Chen, J. Zhong, Y. Ni, D. Gan, J. Xiong, and X. Xia, "Optimal Reactive Power Planning of Radial Distribution Systems with Distributed Generation," *Automation of Electric Power Systems*, vol. 30, no. 14, pp. 20-24, 2006.
[19] Y. Deng, X. Ren, C. Zhao, and D. Zhao, " A Heuristic and Algorithmic Combined Approach for Reactive Power Optimization with Time-varying Load Demand in Distribution Systems," *Power Systems IEEE Transactions on*, vol. 17, no. 4, pp. 1068-1072, 2002.
[20] P. R. Laframboise, G. Ferland, A. Y. Chikhani, and M. M. A. Salama, "An Expert System for Reactive Power Control of a Distribution System. Part 2: System Implementation," *IEEE Transactions on Power Systems*, vol. 10, no. 3, pp. 1433-1441, 1995.
[21] Z. L. Shu, Y. H. Guo, and J. Tang, "Implementation of FPGA Based Three Phase Phase-Locked Loop System," *Power Electronical Technology*, no. 6, pp. 126-128, 2005.
[22] P. Roncero-Sanchez, X. D. T. Garcia, A. P. Torres, and V. Feliu, "Fundamental Positive- and Negative-sequence Estimator for Grid Synchronization under Highly Disturbed Operating Conditions," *IEEE Transactions on Power Electronics*, vol. 28, no. 8, pp. 3733-3746, 2013.
[23] W. Dou, "Current Controller Optimum Design for Three-Phase Photovoltaic Grid-Connected Inverter," *Transactions of China Electrotechnical Society*, vol. 25, no. 8, pp. 85-90, 2010.
[24] X. N. Li, Q. L. Pang, and J. Su, "Three-phase PLL Based on Generalized Rotation Angle," *Proceedings of the CSU-EPSA*, vol. 30, no. 174, pp. 49-54, 2018.
[25] I. Carugati, S. Maestri, P. G. Donato, D. Carrica, and M. Benedetti, "Variable Sampling Period Filter PLL for Distorted Three-phase Systems," *IEEE Transactions on Power Electronics*, vol. 27, no. 1, pp. 321-330, 2012.
[26] E. Zangeneh Bighash, S. M. Sadeghzadeh, E. Ebrahimzadeh, and F. Blaabjerg, "Improving Performance of Lvrt Capability in Single-phase Grid-tied PV Inverters by a Model-predictive Controller," *International Journal of Electrical Power & Energy Systems*, vol. 98, pp. 176-188, 2018.
[27] Y. F. Wang, and Y. W. Li, "Three-phase Cascaded Delayed Signal Cancellation pll for Fast Selective Harmonic Detection," *IEEE Transactions on Industrial Electronics*, vol. 60, no. 4, pp. 1452-1463, 2013.
[28] B. I. Rani, C. K. Aravind, G. S. Ilango, and C. Nagamani, "A Three Phase pll with a Dynamic Feed Forward Frequency Estimator for Synchronization of Grid Connected Converters under Wide Frequency Variations," *International Journal of Electrical Power & Energy Systems*, vol. 41, no. 1, pp. 63-70, 2012.
[29] D. Zhao, N. Zhang, Y. Liu, and X. Zhang, "Synthetical Control Strategy for Smooth Switching between Grid-connected and Islanded Operation Modes of Microgrid Based on Energy Storage System," *Power System Technology*, vol. 37, no. 2, pp. 301-306, 2013.
[30] S. F. Mekhamer, S. A. Soliman, M. A. Moustafa, and M. E. El-Hawary, "Application of Fuzzy Logic for Reactive Power Compensation of Radial Distribution Feeders," *IEEE Power Engineering Review*, vol. 22, no. 11, pp. 58-58, 2002.
[31] J. H. Zheng, Y. T. Wang, X. W. Li, Z. J. Wang, X. Y. Wang, and S. Z. Zhu, "Control Methods and Strategies Microgrid Smooth Switchover," *Automation of Electric Power Systems*, vol. 35, no. 18, pp. 17-24, 2011.
[32] J. H. Zheng, X. W. Li, Y. T. Wang, S. Z. Zhu, X. Y. Wang, and H. B. Zhu, "Small-signal Stability Analysis of a Microgrid Switching to Islanded Mode," *Automation of Electric Power Systems*, vol. 36, no. 15, pp. 25-32, 2012.
[33] T. Zhang, and L. I. Xuxin, "A Control Strategy for Smooth Switching between Island Operation Mode and Grid-connection Operation Mode of Microgrid Containing Photovoltaic Generations," *Power System Technology*, vol. 39, pp. 904-910, 2015.
[34] Y. Fu, L. S. Huang, and J. J. Zhao, "Microgrid Control Strategy for Smooth Mode Transfer Based on Coordination Between Double-fed Induction Generator and Battery," *Proceedings of the CSU-EPSA*, vol. 29, no. 3, pp. 55-61, 2017.
[35] W. H. Cui, J. S. Wang, and Y. Y. Chen, "Design and Performance Testing of Lead-acid Battery Experimental Platform in Energy Storage Power Station," *IAENG International Journal of Computer Science*, vol. 44, no. 4, pp. 471-481, 2017.

Xin-Feng Du is a postgraduate student in the School of Electronic and Information Engineering, University of Science and Technology Liaoning, Anshan, 114051, PR China. His main research interest is modeling and control methods of microgrid.

Shuang Zhao is is an engineer of Anshan Power Supply Company, State Grid Liaoning Electric Power Co. LTD., Anshan, 114051, PR China. Her main research interest is modeling and control methods of microgrid.

Jie-Sheng Wang received his B. Sc. And M. Sc. degrees in control science from University of Science and Technology Liaoning, China in 1999 and 2002, respectively, and his Ph. D. degree in control science from Dalian University of Technology, China in 2006. He is currently a professor and Doctor's Supervisor in School of Electronic and Information Engineering, University of Science and Technology Liaoning. His main research interest is modeling of complex industry process and intelligent control.

An He is an engineer of Anshan Power Supply Company, State Grid Liaoning Electric Power Co. LTD., Anshan, 114051, PR China. His main research interest is modeling and control methods of microgrid.